



HI Galaxy Detections in the Zone of Avoidance with FAST

Chao Feng^{1,2}, Bin Liu¹, Hong-Wei Xi¹, and Bo Peng¹

¹ CAS Key Laboratory of FAST, National Astronomical Observatories, Chinese Academy of Sciences, Beijing 100101, China; pb@bao.ac.cn

² School of Astronomy and Space Science, University of Chinese Academy of Sciences, Beijing 100049, China

Received 2023 April 14; revised 2023 May 23; accepted 2023 May 30; published 2023 July 19

Abstract

The Zone of Avoidance (ZoA) is a region of low galactic latitude that is heavily obscured by the Milky Way. Observations with radio telescopes are basically unaffected by dust extinction and can unveil the structure behind it through the Milky Way. One of the scientific goals of the Five-hundred-meter Aperture Spherical radio Telescope (FAST) is to search for the neutral hydrogen and understand the large-scale physics to explore the origin and evolution of the universe. We take the 15,500 IRAS (the Infrared Astronomical Satellite) galaxies from PSCz (“Point Source Catalog”) survey to reconstruct the density field of the local universe, obtain the distribution of the relative density of galaxies in the ZoA region with a redshift z below 0.07, and the number of detectable galaxies with FAST is estimated by using the neutral hydrogen mass function of the ALFA (Arecibo L -band Feed Array) survey. We conclude that FAST can observe more than 2000 ZoA galaxies within a distance of 300 Mpc h_{70}^{-1} , and present preliminary results of the partial GPPS (the FAST Galactic Plane Pulsar Snapshot survey) data, compared with ALFA ZoA (The Arecibo L -band Feed Array Zone of Avoidance), show that FAST has a higher detection sensitivity to search for HI galaxies in the ZoA area.

Key words: galaxies: distances and redshifts – (cosmology:) large-scale structure of universe – surveys

1. Introduction

Optical and near-infrared (NIR) observations are heavily extinct in a region, referred as the Zone of Avoidance (ZoA), due to the high density of dust and stars in the Milky Way, which results in the loss of 10%–20% of the astrophysical and large-scale structural information in various all-sky surveys. In recent years, ZoA has been studied by many sky surveys in an attempt to fill up the cognitive gap between this region and others. The extinction of stars and dust at optical wavelengths in the Milky Way causes significant confusion. The extinction at longer wavelengths is less obvious. Surveys in the infrared, like the Infrared Astronomical Satellite (IRAS) (Soifer et al. 1987) and the Two Micron All-Sky Survey (2MASS) (Huchra et al. 2012), have presented us a more complete map of the distribution of galaxies in the sky. In the neutral hydrogen 21 cm band, the Milky Way is almost transparent, it is better to use radio telescopes to investigate the region behind the Milky Way.

The Dwingeloo Obscured Galaxies Survey (DOGS) is a HI blind survey of the ZoA in the northern sky with the Dwingeloo 25 m radio telescope. A total of 36 galaxies were discovered, of which 23 have no counterparts (Rivers et al. 1999). The Parkes HI ZoA survey detected 883 galaxies with a redshift below 0.04 in the southern sky of 1760 square degrees. By mapping these galaxy samples, the large-scale structural distribution of the low galactic latitude can be obtained, Like Puppis, Great Attractor regions, and the Local Void are presented, and some new structures are revealed as well (Staveley-Smith et al. 2016).

Combining these data with near-infrared observations to obtain accurate distance and location distributions from the Tully Fisher relationship, the density and velocity fields of the ZoA region can be made, which is of great significance for understanding the dynamics of local groups. The Arecibo L -band Feed Array Zone of Avoidance Shallow Survey is currently the complete HI survey for the ZoA area in the northern sky. It conducted a neutral hydrogen blind survey in an area of 1360 square degrees with extremely high sensitivity, detected 403 galaxies with a redshift velocities of $12,000 \text{ km s}^{-1}$, authenticated locations of large-scale structures such as C7, C ζ , Pegasus, Corona Borealis, and Delphinus structures (Sanchez-Barrantes et al. 2019), and further refined our understanding of the local universe.

The Five-hundred-meter Aperture Spherical radio Telescope (FAST) in Guizhou, China is currently the largest single-dish radio telescope. One of its scientific goals is to conduct a large-scale neutral hydrogen survey to form high-quality images of neutral hydrogen in sky. FAST relies on the installation of 19-beam receivers and extremely high sensitivity, allows high-quality, high-efficiency survey for extragalactic neutral hydrogen galaxies. It is expected to discover fainter galaxies in the ZoA region and make up for the missing information in the ZoA area. In this paper, IRAS galaxies are used as samples to construct the galaxy density field in the ZoA region, combined with FAST’s performance parameters to estimate HI galaxy detections.

This paper can be divided into the following parts: Section 2.1 is the method of simulation we adopt in paper, we briefly

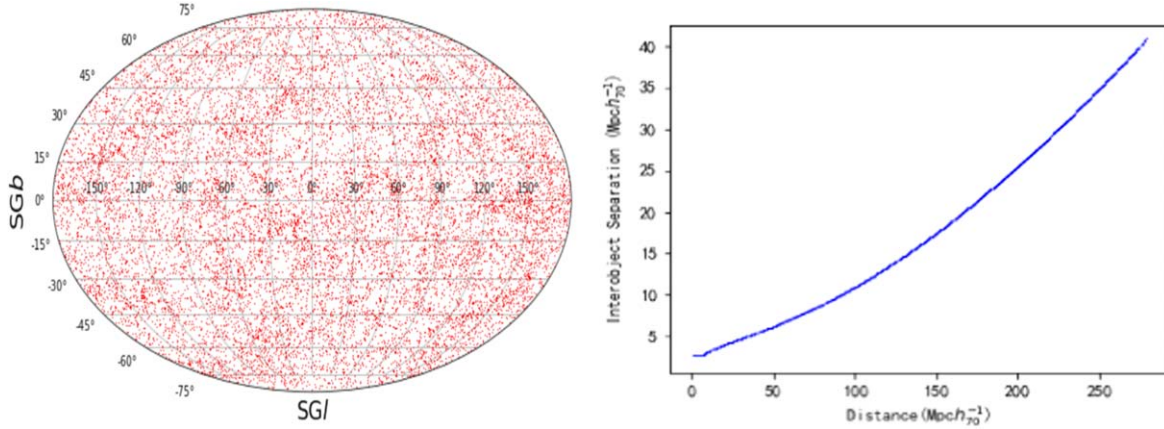


Figure 1. Left panel: Aitoff projection of the galaxy distribution in supergalactic coordinates in the PSCz survey. Right panel: Mean inter-object separation as a function of radial distance.

introduce the galaxies data and main parameters used to estimate the density field in Sections 2.2, 2.3 is the data processing and the main results. In Section 3, we present some basic parameters of GPPS (the FAST Galactic Plane Pulsar Snapshot survey) observations and preliminary results of GPPS data processing. Finally, we make a summary of the predicted work in Section 4, we adopt H_0 (Hubble constant) = $70 h_{70} \text{ km s}^{-1} \text{ Mpc}^{-1}$, Ω_m (density parameter of matter) = 0.3 and Ω_Λ (density parameter of dark energy) = 0.7 in this paper.

2. Simulation

2.1. The Method of Simulation

Through density analysis, we can generate a continuous surface from the measured data points, and could find out where the points are relatively concentrated. Density analysis calculates the aggregation of data over an entire area based on input data, and it is also the process of interpolation for discrete data point. According to different interpolation principles (Węglarczyk 2018), density analysis is mainly divided into ordinary density analysis and kernel density analysis. In ordinary density analysis, points falling within the search area have the same weight, which are summed first and then divided by the size of the search area to obtain the density value of each point. In kernel density analysis, the points falling into the search area have different weights, which are assigned higher for the points close to the search center. On the contrary, the weights are smaller, and the distribution of the simulated results is smoother, kernel density is also the method adopted in this paper.

2.2. The Data

The data used in this article are mainly from the IRAS galaxies sample of the PSCz (“Point Source Catalog”) redshift survey, including 15 500 galaxies with recession velocities below $30,000 \text{ km s}^{-1}$ and a $60 \mu\text{m}$ flux, $f_{60} > 0.6 \text{ Jy}$, covering

about 84% of the sky. The sky projection of these galaxies in the galactic coordinate is shown in Figure 1. Affected by the large-scale structure, the number of galaxies one can observe at different redshifts is also different, with the expansion of the observation area, the number of galaxies observable in the low-redshift range generally appear an upward trend with the increase of distance, however, the flux limit of the telescope at the high redshift decreases rapidly with distance, and the number of detectable galaxies decreases with distance. Therefore, when estimating the number of galaxies at different distances, it is necessary to define a selection function $\phi(r)$ to correct the impact of the selection effect on the observation, r is the distance given by $r = cz/H_0$. The $\phi(r)$ is given by Yahil et al. (1991) in maximum-likelihood techniques as the following equation

$$\phi(r) = Ar^{-2\alpha} \left(\frac{1+r^2}{r_*^2} \right)^{-\beta} \text{ if } r > r_s. \quad (1)$$

A in the formula is constant, $r_s = 6 \text{ Mpc } h_{70}^{-1}$, according to the work (Branchini et al. 1999), the values of the parameters have been given as $\alpha = 0.52$, $\beta = 1.92$, $r_* = 90.75 \text{ Mpc } h_{70}^{-1}$, and at the same time, we set $\phi(r) = 1$ at $r < r_s$, to avoid assigning excessive weight to nearby galaxies. Table 1 is an example page of the catalog, which lists the basic information of each galaxy, and each column is described as follows:

Column (1)—redshift in LG (Local Group) frame (km s^{-1});
Column (2), (3), (4)—SGX, SGY, SGZ, a component of the reconstructed positions in space (supergalactic coordinates);
Column (5), (6), (7)—Cartesian component of the Peculiar velocity vectors (in supergalactic coordinates);
Column (8) - component V_{pec} in the LG frame;
Column (9) - Statistical weight that corrects for magnitude limited selection, which is the inverse of the selection function at that redshift.

Table 1
IRAS Galaxies Parameters in the Sample

Recession velocities (km s ⁻¹)	SGX Mpc h ₇₀ ⁻¹	SGY Mpc h ₇₀ ⁻¹	SGZ Mpc h ₇₀ ⁻¹	V _{Px} (km s ⁻¹)	V _{Py} (km s ⁻¹)	V _{Pz} (km s ⁻¹)	V _{Pec} (km s ⁻¹)	Weight ($\phi(r)$) ⁻¹
11864.39	102.03	18.48	33.63	404.91	-547.11	-211.42	964.00	106.38
10638.16	90.64	22.36	29.56	369.64	-407.88	-327.91	845.41	75.43
4530.69	40.20	13.12	13.44	-178.52	-146.61	-1107.93	93.20	11.21
1959.50	17.48	6.16	5.32	-405.76	176.00	-876.09	31.69	3.45
16871.78	145.06	57.13	42.24	557.07	-451.82	-492.99	719.24	441.83
27606.10	226.06	87.79	73.36	1329.73	663.78	372.32	2270.22	2851.71
11007.70	91.38	37.22	30.74	244.07	-53.95	-316.70	672.90	89.43
5414.70	47.87	23.18	14.68	-294.30	-240.41	-909.97	-102.97	17.08
5426.28	46.40	23.57	16.76	-213.31	-200.75	-924.77	-41.69	16.77
5027.54	44.25	22.72	13.37	-204.69	-371.02	-986.75	-123.32	14.85
6167.14	53.80	29.00	16.68	-518.78	-98.31	-569.81	-168.28	23.17
24835.58	202.03	102.57	54.87	1120.13	40.99	189.57	1522.87	1992.77
4793.00	44.09	16.84	12.21	-341.42	-99.91	-1168.70	-81.91	13.34
1453.95	12.23	4.86	3.42	-378.33	285.12	-807.57	94.25	2.33
5831.85	55.42	21.07	13.96	-615.19	-110.23	-862.00	-258.89	21.17
5800.98	54.75	21.77	14.09	-612.79	-100.90	-843.59	-256.76	20.92

Obtaining this basic information, we can divide the entire real space into several cubes of unit volume size and smooth them in Gaussian, so that the density of the number of galaxies at a point in space can be expressed by the number of galaxies in the cube where it is located,

$$\langle n \rangle = \frac{1}{V} \sum_{i=1}^{N_g} (\phi(r_i))^{-1}, \quad (2)$$

where V is the volume of the sample and $\phi(r_i)$ is the selection function at r_i .

2.3. The Results of Simulation

We consider galaxies with redshift within $120 \text{ Mpc } h_{70}^{-1}$, divide the entire space into 64^3 volume elements, display the weights of these galaxies in the galaxy distribution scatter with color bar in Figure 2, use a Gaussian filter with a smoothing length of $6 \text{ Mpc } h_{70}^{-1}$ at $r = 80 \text{ Mpc } h_{70}^{-1}$ according to $R_{\text{Smoothing}} = l(r) = [\phi(r) \langle n \rangle]^{-1/3}$ for Gaussian smoothing, and we can obtain the galaxy density distribution at the $\text{SGZ} = 0$ plane. $l(r)$ is the mean inter-object separation, as a function of r , which has been shown in the right panel of Figure 1. Due to the Hubble's expansion, the minimum separation between objects will increase with the increasing observing distance. We use the mean inter-object separation as natural smoothing length to keep the shot noise at a constant level.

As we can see in Figure 3: the Local Supercluster centered on the Virgo Cluster [(SGX, SGY) = (-2.5, 11.5)] is the largest and second brightest structure, which is related to both the Hydra Centaur Supercluster [(SGX, SGY) = (-35, 20)] and the Great Attractor [(SGX, SGY) = (-40, 15)]. There are several highest overdensity structures at the bottom right of the figure, and the

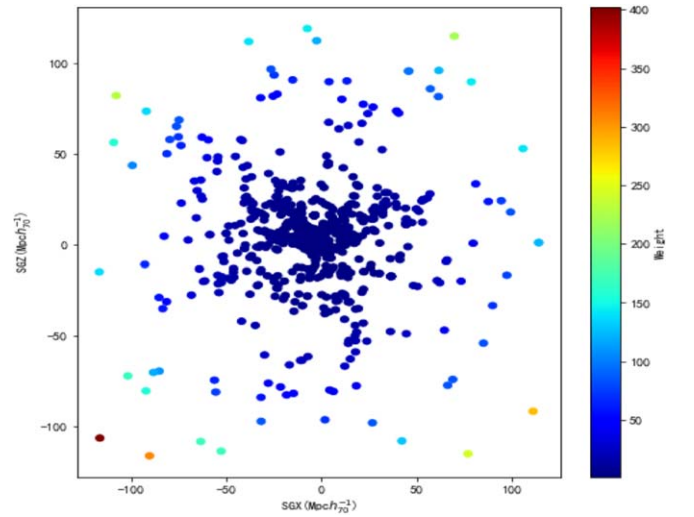


Figure 2. At the $\text{SGZ} = 0$ plane, IRAS galaxies within $120 \text{ Mpc } h_{70}^{-1}$ are distributed in SGX-SGY supergalactic coordinates, and different colors represent different weights $(\phi(r))^{-1}$.

ZoA region not only passes through the Local Supercluster but also has large-scale structures such as [(SGX, SGY) = (-100, 0)], [(SGX, SGY) = (70, 0)] elsewhere.

3. Discussion

3.1. Relevant Parameters of FAST

The FAST Galactic Plane Pulsar Snapshot survey (Han et al. 2021) is a search project for pulsars in the galactic plane. At the same time, the pulsar back-end and spectral back-end are applied to take the data. Our neutral hydrogen spectrum data is based on

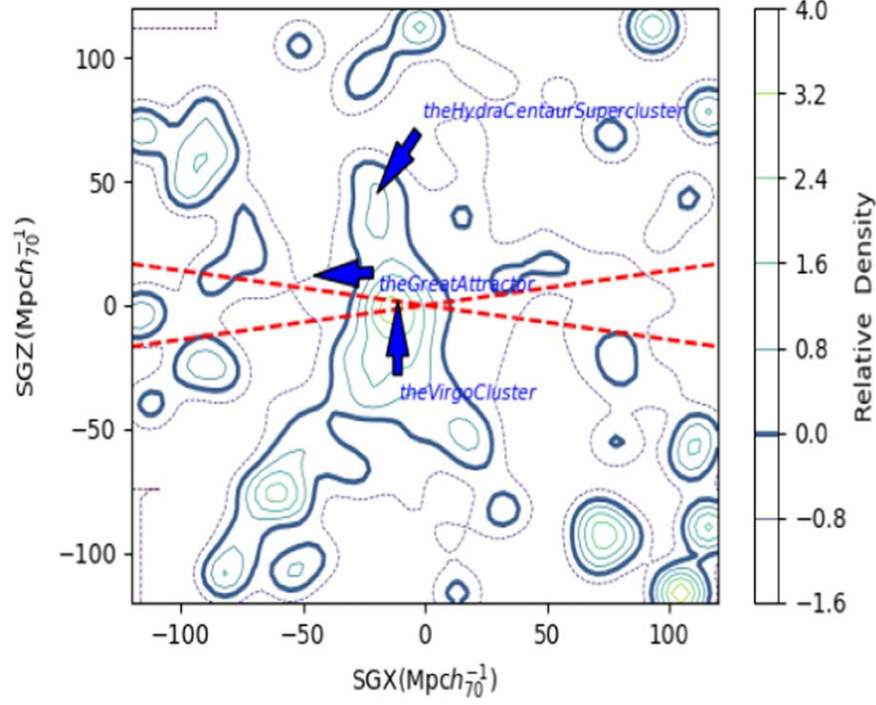


Figure 3. The true space density field at $SGZ = 0$ constructed by the PSCz galaxies, which is smoothed by Gaussian filter with a smoothing length of $6 \text{ Mpc } h_{70}^{-1}$. The contour line represents the space relative density δ , which is actual density minus average density, the thickened solid line in the figure is the contour line of $\delta = 0$, and the solid and dashed contours are the regions of $\delta > 0$ and $\delta < 0$, the red dashed lines is the region where the ZoA is located.

Table 2
Some Observation Parameters of FAST GPPS Survey

Parameter	Value
FAST location: latitude	N 25°647
FAST location: longitude	E 106°856
Effective aperture diameter	300 m
Beam size	3'
Aperture efficiency	60 %
Beam number for a cover	4×19
T_{sys}	$\sim 17.9 \text{ K}$
Telescope gain	$\sim 16 \text{ K Jy}^{-1}$
Zenith angle limit for a full gain	< 26.4
Obs. freq. range	1.0–1.5 GHz
Freq. channel number	1,048,576
Freq. resolution	476.81 Hz
Linear polarizations	XX*, YY*
Sampling time τ_{sampling}	49.152 μs
Survey integration time t_s	300 s

the observation of spectral back-end. Currently, the released GPPS data covers a part of the ZoA region. Some of its main observational parameters are given in Table 2: FAST is located at 25°647 north latitude and 106°856 east longitude, The range of observable sky area is $-0.9 < \text{Decl.} < 52.2$, observational zenith angle at full gain is less than 26.4. The effective

observation diameter is 300 m. In the 19-beam receiver data, the frequency coverage of the L-band is 1.0–1.5 GHz, containing two linear polarizations. Different frequency channels can be selected according to different observational requirements.

The sensitivity of the telescope is related to the integration time t_s , system temperature T_{sys} , frequency resolution Δf_{ch} , gain G , and other related physical quantities. The following formula gives the quantitative relationship (Giovannelli & Haynes 2016)

$$S_{\text{rms}} = \frac{T_{\text{sys}}}{G} \frac{1}{\sqrt{2f_t \Delta f_{\text{ch}} t_s}}. \quad (3)$$

The factor f_t is determined by observation details, such as spectral line smoothing and bandpass subtraction, we adopt $f_t = 0.7$, consistent with ALFA ZoA. In Figure 4, we demonstrated the noise distribution of the 1300–1420 MHz band from the GPPS observation data. It can be seen that the noise in the 1340–1380 MHz band is relatively low, and relatively high at both ends. The average noise in this band is 0.75 mJy.

Assuming that the detected signal is 5 times higher than the baseline noise S_{rms} , that is, $S_{\text{peak}} = 5S_{\text{rms}}$, the following formula can give the minimum HI detection mass (Meyer et al. 2017)

$$\left(\frac{M_{\text{HI}}}{h_{70}^{-2} M_{\odot}} \right) \approx 49.7 \left(\frac{D_L}{h_{70}^{-1} \text{ Mpc}} \right)^2 \left(\frac{S_{\text{int}}}{\text{JyHz}} \right). \quad (4)$$

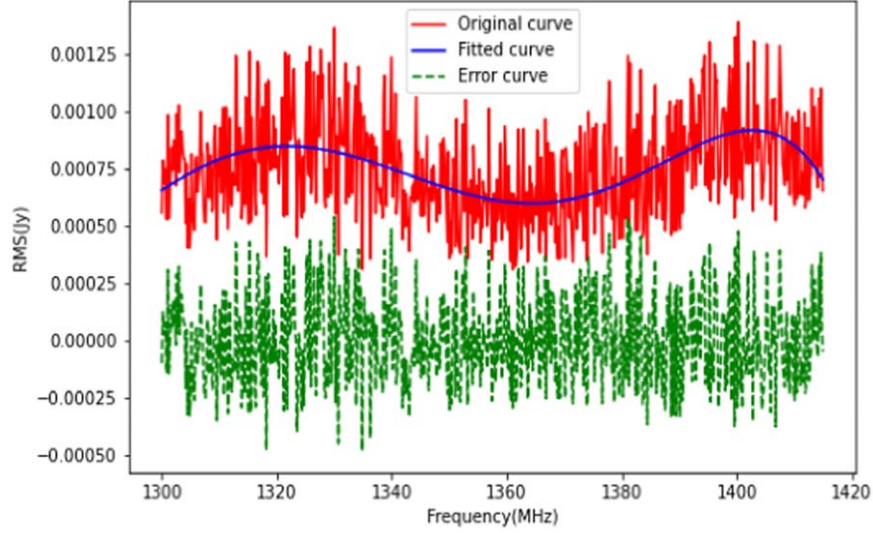


Figure 4. The noise distribution of GPPS data in the 1300–1420 MHz band, the red solid line is the data curve, the blue solid line is the polynomial fitting curve, and the green dotted line is the error curve. The frequency resolution of the data in the figure is 7.629 KHz, and the number of frequency channels in the L -band is 65,536, we generally use this value to process spectral data.

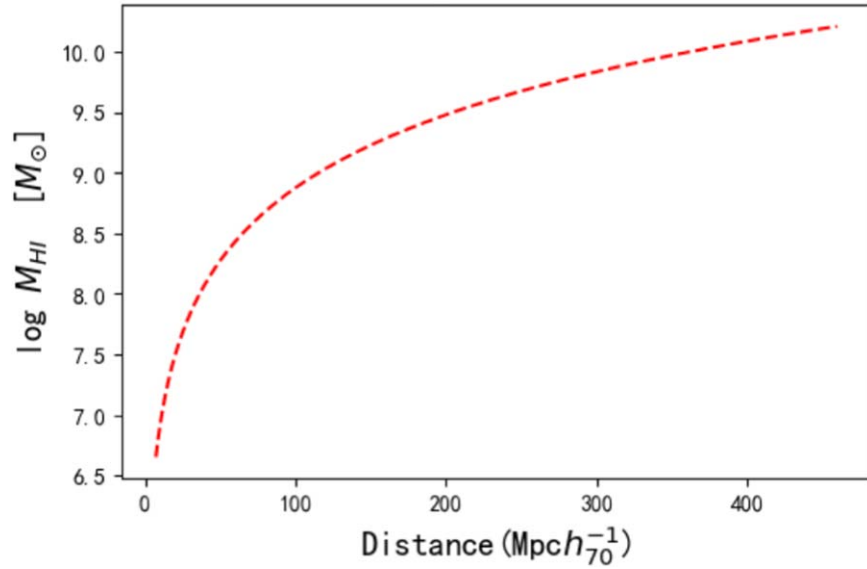


Figure 5. The detection limit of FAST, the horizontal axis is the common motion distance, and the vertical axis is the minimum detectable mass, the S_{int} obtained from Table 2 is 3 mJy.

Where D_L is the luminosity distance and M_{HI} is the lower limit of detectable mass. The function is shown in Figure 5, obviously, with the increase of the distance, the mass of the minimum neutral hydrogen galaxy that can be observed will be larger due to the decrease of the observational flux.

3.2. Comparison of Results

After obtaining the detection limit, we use the neutral hydrogen mass function (HIMF) as the selection function to

estimate the upper limit of the number of detectable galaxies, and HIMF can be described by Schechter functions (Schechter 1976),

$$\Phi(M_{\text{HI}}) = \ln 10 \Phi^* \left(\frac{M_{\text{HI}}}{M_*} \right)^{\alpha+1} e^{-\frac{M_{\text{HI}}}{M_*}}, \quad (5)$$

its three key parameters are the slope of the low mass end α , the characteristic mass M_* , and the normalized parameter Φ^* . It gives the density distribution of galaxies with different neutral

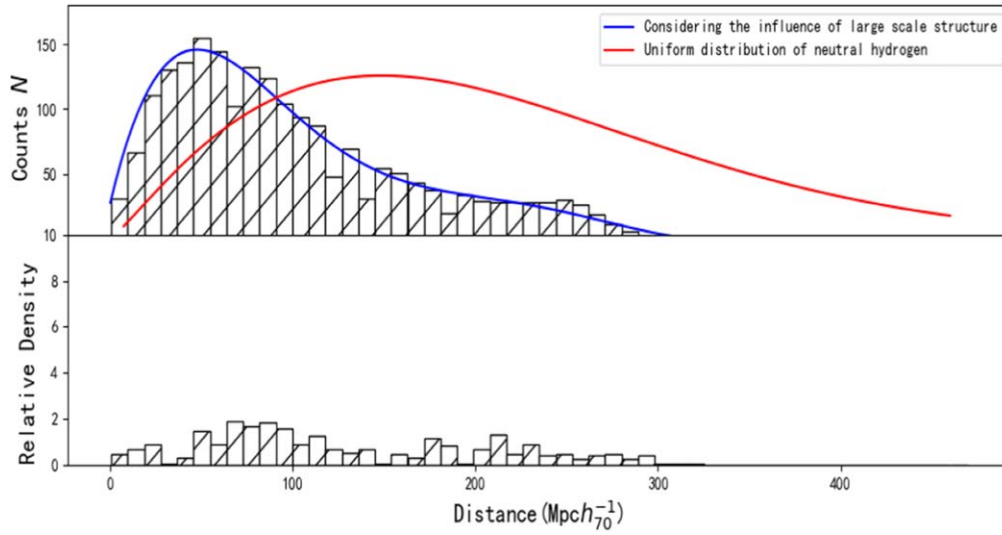


Figure 6. Upper panel: The histogram is the distribution of galaxies in the ZoA region with redshift distance obtained by Monte Carlo sampling, the blue solid line is the best-fit curve of these graphs. The red curve is the galaxy distribution calculated by HIMF given by ALFA without the effect of large-scale structure. Lower panel: Distribution of relative density of galaxy number with distance.

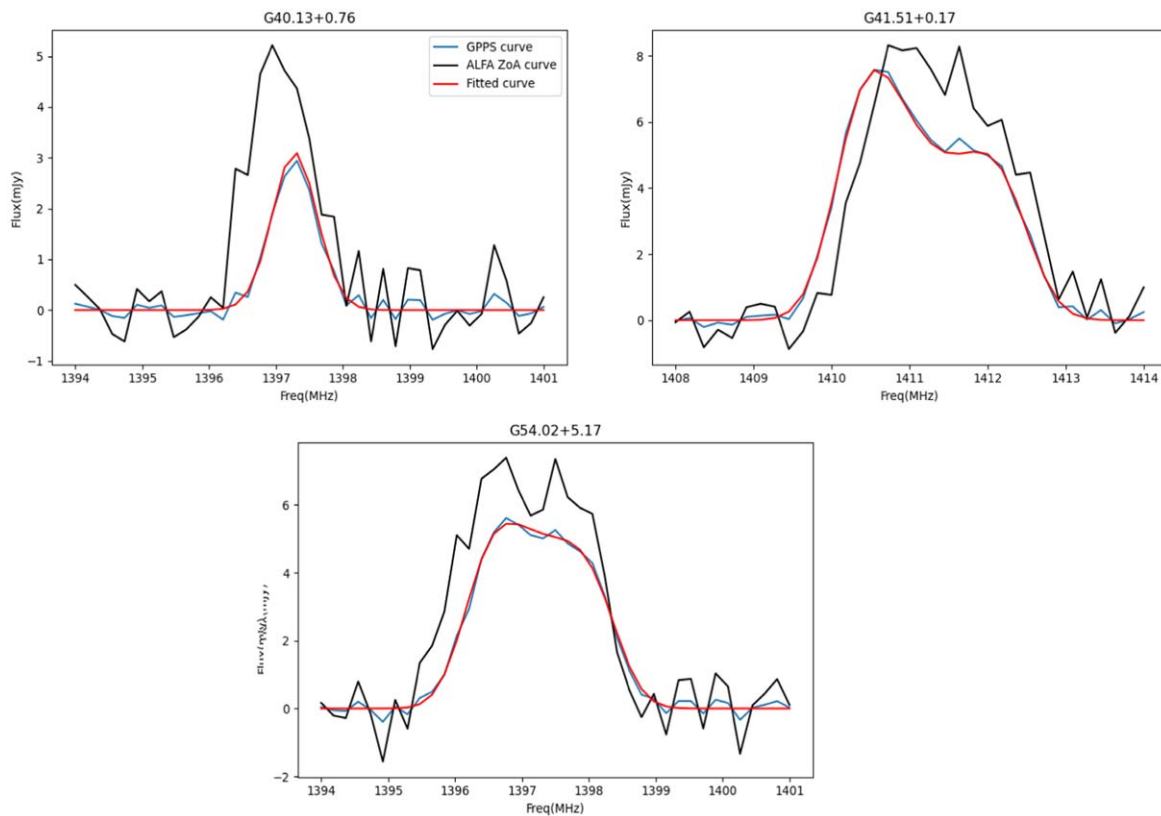


Figure 7. Several H I spectral images of galaxies detected from ALFA ZoA and FAST GPPS.

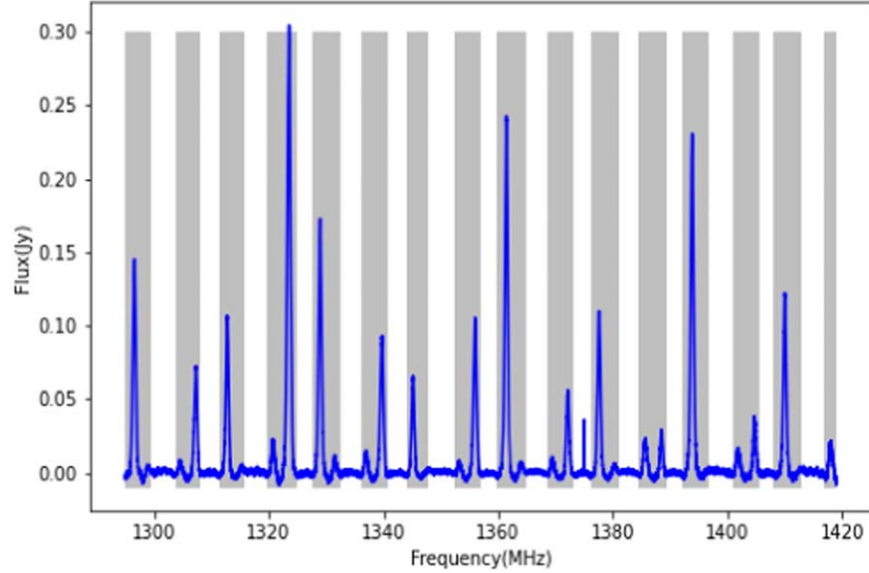


Figure 8. GPPS data in the 1300–1420 MHz band are displayed, and the shaded area marks the receiver compressor RFI with a period of 8.1MHz.

hydrogen mass intervals as a criterion to evaluate the completeness of the survey for neutral hydrogen galaxies, and there are two methods to evaluate the neutral hydrogen mass function: the $\Sigma 1/V_{\max}$ method (Schmidt 1968) and the 2D stepwise maximum likelihood (2DSWML) (Zwaan et al. 2003). Some work has given the values of parameters (Zwaan et al. 2005; Martin et al. 2010; Hoppmann et al. 2015), we directly use the results given by Xi et al. (2021) to obtain the distribution of the number of galaxies observed in the ZoA region, as shown by the solid red line in Figure 6. Considering the influence of the large-scale structure leading to an inhomogeneous distribution of neutral hydrogen, we construct the distribution of galaxies in the ZoA region using Monte Carlo simulations weighted by relative density. Before considering the influence of large-scale structure, fewer galaxies can be detected at close distances in the expected results, and the distance to achieve the maximum number of detectable galaxies is farther, the distribution curve is relatively flat. The distribution curve of Monte Carlo simulations in Figure 6 represents the number of observable galaxies at different distances, by summing the distances, the total number of observable galaxies within a certain observation range can be obtained. Under the observation conditions of FAST GPPS, more than 2000 ZoA galaxies can be observed within the range of $300 \text{ Mpc } h_{70}^{-1}$. In addition, we also give the relative number density of galaxies in the ZoA region as demonstrated in the lower panel of Figure 6. The relative density at $50\text{--}100 \text{ Mpc } h_{70}^{-1}$ is higher, where there may be some overdensity structures, and the relatively low density at $30, 160, 200 \text{ Mpc } h_{70}^{-1}$ corresponds to some void structures.

We selected some ALFA ZoA galaxies as test galaxies to verify the observational performance of FAST, Figure 7 are the HI spectral images of several galaxies. The black solid line is the

data spectrum of ALFA ZoA, and the blue solid line is the data spectrum of FAST GPPS. The number of original frequency channels of FAST GPPS data is 1,048,576. In order to compare with ALFA ZoA data, we reduced the number of channels to 4096 to achieve the same frequency resolution as ALFA ZoA, and also reduced the noise of the data. Under the same frequency resolution, the noise of FAST GPPS is smaller than that of ALFA ZoA, the average value of rms is 0.11 mJy, while the average value of rms of ALFA ZoA is 0.42 mJy, and the peak flux of FAST GPPS data spectrum is also obviously weaker. The red solid line is the curve fitted by busy function (Westmeier et al. 2014), and the definition of busy function is

$$B(x) = \frac{a}{4} \times (\text{erf}[b_1\{w + x - x_c\}] + 1) \times (\text{erf}[b_2\{w - x + x_c\}] + 1) \times (c|x - x_p|^n + 1). \quad (6)$$

The function consists of the product of two error functions and a polynomial function, it mainly includes the following parameters: a is the amplitude of the entire function, the offset of the two error functions and the polynomial function x_c, x_p , the slopes of the two error functions and the polynomial function b_1, b_2, c , the order of the polynomial function n .

By the way, the data of ALFA ZoA that we can obtain is the data cube containing the recession velocities. In our program, the process of converting velocities into frequency only considers the motion of the Local Group, and lacks the solar system and Earth's motion information, resulting in a positional bias in the spectrum. The deviation of the flux may be due to the fact that we only use the relationship between the gain and the zenith angle for rough flux calibration, we need make more observations on the calibration source to obtain accurate flux information.

4. Conclusion

In this paper, we reconstructed the density field of the local universe using a sample of galaxies from the PSCz survey, and obtained the distribution of galaxy density with redshift distance, through using Monte Carlo sampling to simulate the galaxy distribution in the ZoA region, it is not consistent with the results we assume a uniform distribution of neutral hydrogen, which is likely due to the insufficient number of samples that the randomness of the large-scale structure dominates. Under the observation conditions of FAST GPPS, we made a preliminary prediction of the observable galaxy number below a distance of $300 \text{ Mpc } h_{70}^{-1}$, more than 2000 neutral hydrogen galaxies can be observed. Furthermore, factors such as confusion and radio frequency interference (RFI) are not considered, the RFI caused by the receiver compressor of the FAST were demonstrated in Figure 8, about 58% of the frequency range is affected in the 1300–1420 MHz band, and galaxies in these bands are difficult to identify.

In our existing GPPS data, we conducted pilot investigations on 25 ALFA ZoA galaxies, observed five known galaxies, about 70% (18) of the galaxies are in the band with the RFI, and there are two galaxies undetected. The data of current study on the ZoA region are mainly from the survey projects of near-infrared and radio observations. As a radio telescope with excellent performance, FAST is expected to be powerful in this field. More new galaxies and structures will be discovered in the region, to improve theories of cosmology.

Acknowledgments

The data used in this work mainly come from the PSCz sky survey project held by E.Branchini, Department of Physics, University of Durham, South Road, Durham DH1 3LE, and the GPPS sky survey project of the National Astronomical Observatories of the Chinese Academy of Sciences (NAOC).

References

- Branchini, E., Teodoro, L., Frenk, C., et al. 1999, *MNRAS*, **308**, 1
 Giovanelli, R., & Haynes, M. P. 2016, *A&ARv*, **24**, 1
 Han, J., Wang, C., Wang, P., et al. 2021, *RAA*, **21**, 107
 Hoppmann, L., Staveley-Smith, L., Freudling, W., et al. 2015, *MNRAS*, **452**, 3726
 Huchra, J. P., Macri, L. M., Masters, K. L., et al. 2012, *ApJS*, **199**, 26
 Martin, A. M., Papastergis, E., Giovanelli, R., et al. 2010, *ApJ*, **723**, 1359
 Meyer, M., Robotham, A., Obreschkow, D., et al. 2017, *PASA*, **34**, e052
 Rivers, A., Krann-Korteweg, R., & Henning, P. 1999, *PASA*, **16**, 48
 Sanchez-Barrantes, M., Henning, P. A., McIntyre, T., et al. 2019, *ApJ*, **158**, 234
 Schechter, P. 1976, *ApJ*, **203**, 297
 Schmidt, M. 1968, *ApJ*, **151**, 393
 Soifer, B., Houck, J., & Neugebauer, G. 1987, *ARA&A*, **25**, 187
 Staveley-Smith, L., Kraan-Korteweg, R. C., Schröder, A., et al. 2016, *ApJ*, **151**, 52
 Westmeier, T., Jurek, R., Obreschkow, D., Koribalski, B. S., & Staveley-Smith, L. 2014, *MNRAS*, **438**, 1176
 Węglarczyk, S. 2018, *ITM Web of Conferences*, **23**, 00037
 Xi, H., Staveley-Smith, L., For, B.-Q., et al. 2021, *MNRAS*, **501**, 4550
 Yahil, A., Strauss, M. A., Davis, M., & Huchra, J. P. 1991, *ApJ*, **372**, 380
 Zwaan, M. A., Meyer, M., Staveley-Smith, L., & Webster, R. 2005, *MNRAS Lett.*, **359**, L30
 Zwaan, M. A., Staveley-Smith, L., Koribalski, B. S., et al. 2003, *AJ*, **125**, 2842